mater.scichina.com link.springer.com

Published online 9 May 2023 | https://doi.org/10.1007/s40843-023-2438-6
Sci China Mater 2023, 66(8): 3139–3145

Cobalt phosphide nanofibers derived from metal-organic framework composites for oxygen and hydrogen evolutions

Lianli Zou[1,4], Yong-Sheng Wei[1], Qiuju Wang[4], Zheng Liu[2], Qiang Xu[1,3,5*] and Susumu Kitagawa[1,3*]

ABSTRACT **The fabrication of one-dimensional (1D) nanocatalysts with high active surface areas is very important to the development of high-performance catalysts but challenging. Through the phosphidation of metal-organic framework (MOF) nanofiber (NF) composites, bifunctional cobalt phosphide NFs (CoP NFs) which showed a diameter of about 100 nm and length of several micrometers as well as a large catalytic surface area were successfully fabricated and used as the electrocatalysts for water splitting. Taking the advantage of this MOF-derived strategy, a series of 1D nanostructures including Co_3O_4 NFs, and carbon NFs immobilized with CoP or Co nanoparticles were also synthesized and investigated. The density of active sites and catalytic performances of CoP NFs could be improved by the modulation of Cu-related species. The uniform Cu-doped CoP NFs showed the best catalytic performances for both oxygen and hydrogen evolutions with the overpotentials of 330 and 170 mV, respectively, which are comparable to those of commercial noble-metal catalysts. This work provides a facile process to fabricate 1D bifunctional electrocatalysts with desired functionalities for energy-related applications.**

Keywords: cobalt phosphide, electrocatalysis, nanofibers, oxygen evolution reaction, hydrogen evolution reaction

INTRODUCTION

Electrochemical water splitting is an effective approach for renewable energy generation, while the synthesis of high-performance electrocatalysts is challenging [1–4]. Sluggish kinetics on catalysts is the main problem for both oxygen evolution reaction (OER) and hydrogen evolution reaction (HER) during water splitting. To date, the most efficient electrocatalysts for OER and HER are noble-metal catalysts, such as Pt-, Ru- or Ir-based materials, while these catalysts usually suffer from scarcity, high cost and poor stability [5,6]. Transition metal phosphides, which are considered as the most promising candidates to replace noble metals in electrocatalysis systems, have been extensively studied in recent years owing to their relatively high activity, easy synthesis, and low cost with earth abundance [7–10]. As a member of metal phosphides, cobalt phosphide (CoP) shows a wide-pH activity for electrocatalytic reactions, but the intrinsic poor conductivity and durability of CoP nanostructures hinder their practical applications in energy storage and conversion [11–13].

Generally, the catalytic performances of electrocatalysts strongly depend on their compositions and morphologies, as well as the accessible active sites on the surface [4,14–17]. Doping or immobilizing a second active species on the catalyst is an effective method to improve their intrinsic activities. CoP nanocatalysts modulated by other transition metal species could significantly enhance their electrochemical performances through a synergetic effect [12,18–20]. Constructing CoP nanoparticles (NPs) into specific morphology with well-defined pores or shapes would also improve the catalytic properties by adjusting the utilization of the active surface [21,22]. To optimize the structure of these nanocatalysts, the fabrication of one-dimensional (1D) metal phosphide nanofibers (NFs) seems to be a promising strategy to improve the intrinsic activity owing to the enhancement of the transfer ability for mass and electrons, as well as the unique advantages to prevent the aggregation of nanocatalysts [23,24]. To date, though much effort has been applied to synthesize CoP NFs, efficient approaches to fabricate porous CoP NFs with uniform morphologies and large catalytic surface areas are still challenging.

In the past decade, crystalline metal-organic framework (MOF) nanostructures have been widely used as precursors for the fabrication of functional carbons, metal oxides, metal phosphides and/or their composites with relatively high active surface area [25–28]. The sizes and distribution of metal-based NPs could be controlled by adjusting the pyrolysis conditions [29–31]. Owing to the decomposition of ligands, the resulting carbon species would efficiently prevent the aggregation and growth of NPs, forming a large number of active sites and more accessible surface areas, which finally improved the catalytic activity of catalysts [32,33]. MOF-derived metal phosphides

[1] AIST-Kyoto University Chemical Energy Materials Open Innovation Laboratory (ChEM-OIL), National Institute of Advanced Industrial Science and Technology (AIST), Kyoto 606-8501, Japan
[2] Innovative Functional Materials Research Institute, National Institute of Advanced Industrial Science and Technology (AIST), Aichi 463-8560, Japan
[3] Institute for Integrated Cell-Material Sciences (WPI-iCeMS), Kyoto University, Kyoto 606-8501, Japan
[4] Institute for Advanced Materials, School of Materials Science and Engineering, Jiangsu University, Zhenjiang 212013, China
[5] Shenzhen Key Laboratory of Micro/Nano-Porous Functional Materials (SKLPM), SUSTech-Kyoto University Advanced Energy Materials Joint Innovation Laboratory (SKAEM-JIL), Department of Chemistry and Department of Materials Science and Engineering, Southern University of Science and Technology (SUSTech), Shenzhen 518055, China
* Corresponding authors (emails: xuq@sustech.edu.cn or xu.qiang@icems.kyoto-u.ac.jp (Xu Q); kitagawa@icems.kyoto-u.ac.jp (Kitagawa S))

usually focused on the nanocomposites with phosphide NPs immobilized on carbon-based supports, while the relatively poor instability of carbon under high oxidation potentials restricted their applications in OER [15,33]. To enhance the stability and catalytic surface area of nanocatalysts, we developed a kind of Cu-doped CoP (Cu-CoP) NFs by using MOF NF composites as precursors. The 1D porous Cu-CoP NFs with uniform morphology and high density of active sites on the surface were synthesized *via* a facile pyrolysis-phosphidation process, and showed superb catalytic performances for both OER and HER in alkaline conditions.

EXPERIMENTAL SECTION

Synthesis of Co-MOF-74 NF

The synthesis process of MOF NFs was similar to our previous work [14]. Generally, cobalt(II) acetate tetrahydrate (4.0 g) was first dissolved in a methanol solution (150 mL) under vigorous stirring. Then, a methanol solution (150 mL) containing 2,5-dihydroxyterephthalic acid (1.2 g) was poured into the above solution, and the resulting mixture was stirred for about 4 h at room temperature (RT). The resulting precipitate was collected and washed with methanol two times, followed by water two times and then dispersed in 150 mL H_2O. The mixture was then transferred into two Teflon-lined autoclaves, tightly capped, and placed in an oven at 175°C for 12 h. After cooling to RT, the yellow precipitate was collected and washed with water and methanol. The final product (labeled as Co-MOF-74-NF) was kept in methanol for further use.

Synthesis of MOF-NF@CuPPy

As bimetal-MOF NFs with both Co and Cu are not easy to synthesize, Cu was introduced into the MOF composites by using Cu^{2+} as the oxidant to coat a thin layer of polypyrrole (PPy) on the surface of Co-MOF NFs (MOF-NF@CuPPy). Co-MOF-74-NF (0.2 g) was firstly dispersed in 100 mL H_2O, and 0.4 mL pyrrole was dropped and stirred for about 5 min to form a homogeneous mixture. Afterwards, 50 mL aqueous solution containing 0.68 g $CuCl_2{\cdot}2H_2O$ was added into the above mixture and stirred at RT for about 48 h until its color changed into black. The resulting products (labeled as MOF-NF@CuPPy) were washed with water several times and then dried in a cooling machine for further use.

Synthesis of CoP NF and Cu-CoP NF

The as-prepared Co-MOF-74 NF (or MOF-NF@CuPPy) was transferred into a ceramic boat and placed into a temperature-programmed furnace under air atmosphere. With a heating rate of 2°C min^{-1}, the temperature was increased to 250°C and kept for 2 h before cooling. The resulting black solid was collected and labeled as Co_3O_4 NF or Cu-Co_3O_4 NF. Then, about 0.1 g Co_3O_4 NF (or Cu-Co_3O_4 NF) and 0.3 g NaH_2PO_2 were separately placed into a temperature-programmed furnace under an argon flow with the NaH_2PO_2 at upstream of the flow. The temperature was raised to 300°C with a heating ramp rate of 2°C min^{-1} from RT, and maitained at 300°C for 1 h. After cooling down naturally, the resulting products were collected and labeled as CoP NF (or Cu-CoP NF).

Characterizations

Powder X-ray diffraction (XRD) measurements were performed on a Rigaku Ultima IV X-ray diffractometer with a Cu Kα source (40 kV, 40 mA). Fourier transform infrared spectroscopy (FT-IR) analyses were carried out on a Shimadzu IRTracer-100 in air mode. N_2 adsorption/desorption isotherms were used to analyze the surface areas and pores of the catalysts, which were tested at liquid nitrogen temperature (77 K) after the dehydration under vacuum at 120°C for 12 h using automatic volumetric adsorption equipment (Belsorp-max). X-ray photoelectron spectroscopic (XPS) analyses were conducted on a Shimadzu ESCA-3400 instrument. Morphologies of the catalysts were observed *via* a field-emission scanning electron microscope (FE-SEM, Regulus8200). Transmission electron microscopy (TEM) and high-angle annular dark-field scanning TEM (HAADF-STEM) images were taken by using a JEM-ARM200FC equipped with CEOS Cs correctors at 120 kV. Energy dispersive X-ray spectrometry (EDS) elemental mapping analyses were performed on the JED-2300 attached to the JEM-ARM200FC.

Electrochemical measurements

Electrocatalytic measurements were carried out in a three-electrode cell using a rotating ring-disk electrode (RRDE) with a CHI7088E electrochemical workstation at ambient conditions. A graphite rod and a Ag/AgCl electrode in saturated aqueous KCl solution were used as the counter and reference electrodes, respectively. A catalyst-loaded glassy carbon rotating disk electrode (RDE, 5 mm in diameter, 0.196 cm^2 of geometric surface areas) was used as the working electrode. All potentials in this study refer to reversible hydrogen electrode (RHE, $E_{RHE} = E_{Ag/AgCl} + 0.059pH + 0.198$ V). Catalyst inks were prepared by ultrasonically dispersing 5.0 mg powder into 1.0 mL mixture solution (0.48 mL ethanol, 0.48 mL H_2O and 40 μL 5%-Nafion solution). The mixture was sonicated for about 60 min to form a homogeneous ink. Then, a certain volume of catalyst ink was dropped onto the surface of glassy carbon, giving a loading of 0.4 mg cm^{-2} for all samples. After being dried at RT naturally, the catalyst-loaded electrode was tested in a 1.0 mol L^{-1} KOH aqueous solution. Linear sweep voltammetry (LSV) measurements were conducted at a sweep rate of 10 mV s^{-1}. To value the stability of these samples, the catalysts were loaded on a nickel foam with a geometric surface area of about 0.4 cm^{-2} instead of glassy carbon.

RESULTS AND DISCUSSION

Crystal, morphology and composition characterizations

Crystal structures of these samples were firstly measured by XRD. Co-MOF-74 NF and MOF-NF@CuPPy showed the same diffraction patterns (Fig. S1). After being calcinated in air, most carbon in the samples was removed, forming the composite NFs with Co_3O_4 as the main phase (Fig. 1, Figs S2 and S3). As shown in Fig. 1b, Cu-Co_3O_4 NFs converted into Cu-CoP NFs *via* the phosphidation process. The similar XRD diffraction patterns of CoP and Cu-CoP demonstrated the same crystalline structure of the two samples. N_2 sorption isotherms showed a sharp increase of gas adsorption at the relative pressure of 0.9–1.0, while very weak adsorption was observed between 0 and 0.6, suggesting the meso- or macro-porous structure of these NFs (Fig. 1c) [28]. Brunauer–Emmett–Teller (BET) surface areas of Co_3O_4 NFs and Cu-Co_3O_4 NFs were about 55.8 and 59.5 m^2 g^{-1}, respectively, larger than those of CoP NFs and Cu-CoP NFs with values of 16.1 and 22.9 m^2 g^{-1}, respectively. Consistent with the sorption

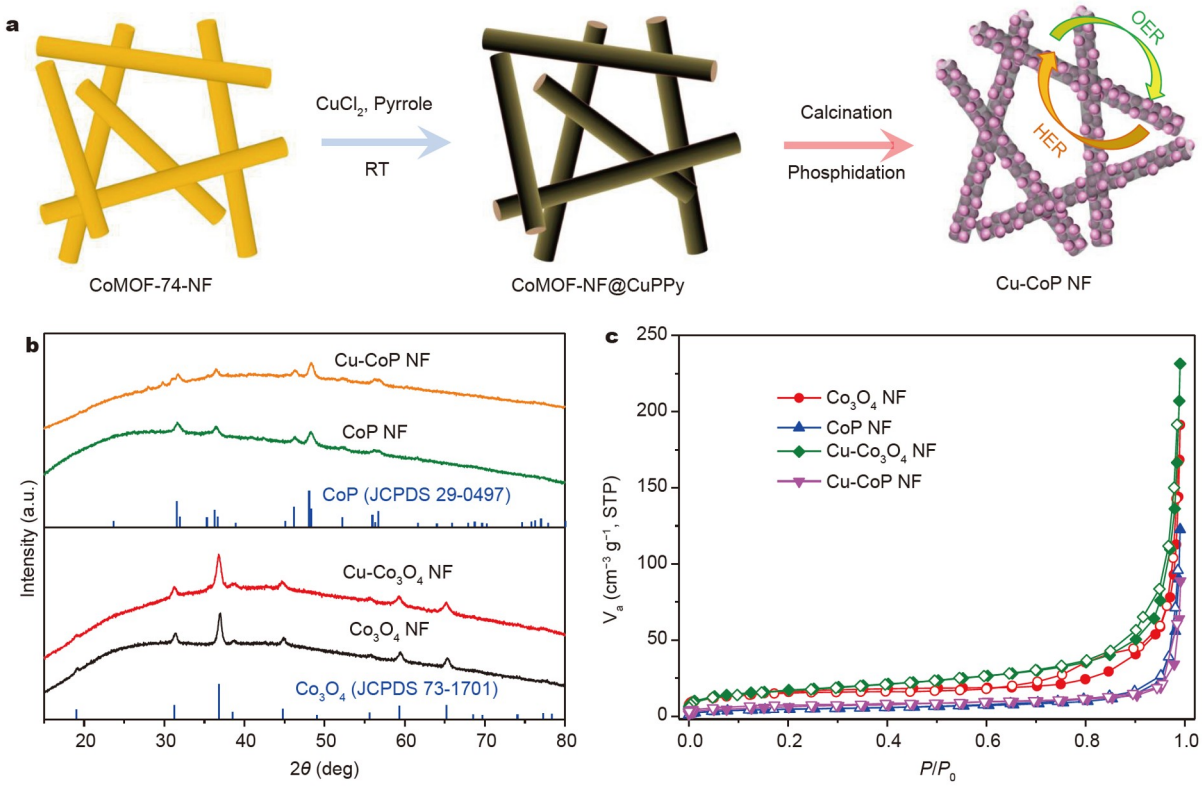

Figure 1 (a) Synthetic strategies for bifunctional Cu-CoP NFs. (b) XRD patterns and (c) N_2 sorption curves of the prepared catalysts.

curves, pore size distribution curves also confirmed the existence of mesopores in these MOF-derived nanocatalysts (Fig. S4, Table S1).

Morphologies of the catalysts were observed by SEM, and all the samples presented a uniform 1D morphology, forming a cross-linked structure (Figs S5–S7). Cu-CoP NFs showed a diameter of about 100 nm, while the length of NFs reached up to several micrometers (Fig. 2a). As observed from the SEM images, there are many pores on the surface of NFs. TEM analysis demonstrated that NFs are composed of tiny CoP NPs, with a small fraction of carbon species (3 wt%) between the slits of these NPs (Fig. 2b, Fig. S8). It is believed that the ligand-derived carbon between Co_3O_4 NPs could efficiently prevent the growth of NPs during the phosphidation process, resulting in the formation of metal–carbon interface with more accessible active sites. HAADF-STEM images displayed that the particle size of Cu-CoP was about 10–20 nm (Fig. 2c). The distance of 0.38 nm is consistent with the interplanar spacing of {101} planes of CoP (Fig. 2d) [34,35]. EDS mapping of a Cu-CoP NF demonstrated the existence of C, N, O, P, Co and Cu in the sample (Fig. 2e). The uniform distribution of Cu along the long axis suggested the successful doping of Cu in CoP NFs.

XPS analysis was used to study the chemical status of the as-prepared samples. Consistent with the EDS mapping results, survey spectrum of Cu-CoP NFs revealed the existence of C, N, O, P, Co and Cu on the surface (Fig. 3a, Fig. S9). The P 2p spectrum could be divided into three peaks, which centered at about 129.0, 130.0, and 134.2 eV, corresponding to the P $2p_{3/2}$, P $2p_{1/2}$ and P–O species, respectively (Fig. 3b). The high intensity of P–O species was ascribed to the superficial oxidation of metal phosphides when exposed to air [11]. In the Co 2p spectrum, peaks located at about 778.6 and 793.7 eV were ascribed to Co $2p_{3/2}$ and Co $2p_{1/2}$ for Co–P bonds, while the peaks at about 782.5 and 798.5 eV corresponded to the oxidation peaks of Co owing to the partially oxidized Co species on the surface (Fig. 3c) [22]. Compared with CoP NFs, the Co–P bands in Cu-CoP NFs showed a relatively high binding energy with a value of about 0.2 eV, suggesting that Cu doping could effectively tune the electronic structure of CoP. As shown in Fig. 3d, the Cu 2p spectrum showed two obvious peaks at 932.5 and 952.6 eV, corresponding to the Cu–P bonds [19,20]. Similar results were observed in CoP NFs except for the absence of N and Cu-related species (Fig. S10).

OER

Catalytic activities toward OER of the as-prepared samples were measured in a 1.0 mol L^{-1} KOH aqueous solution. Owing to the highly active metal phosphides with well-defined morphologies, LSV curves showed that Cu-CoP NFs presented the best OER performance with an overpotential of 330 mV at 10 mA cm^{-2} (Fig. 4a, b), smaller than those of Cu-Co_3O_4 NFs (357 mV), Co_3O_4 NFs (409 mV), CoP NFs (373 mV), and commercial RuO_2 (424 mV), which was also comparable to those of very recently reported results, such as S-doped NiFe-layered double hydroxide (LDH) [36], yolk-like Mn-Co-Se [37], CoP-carbon nanotube [38] and Cu_3P nanoarrays on a conductive support [39]. The Tafel slope of Cu-CoP NF was about 102 mV dec^{-1}, much superior to the commercial RuO_2 (165 mV dec^{-1}), suggesting the great potential of this kind of nanocatalysts (Fig. 4c). To have further insights into the intrinsic activity of electrocatalysts, BET-normalized polarization curves were carried out and Cu-CoP NFs exhibited the highest current density com-

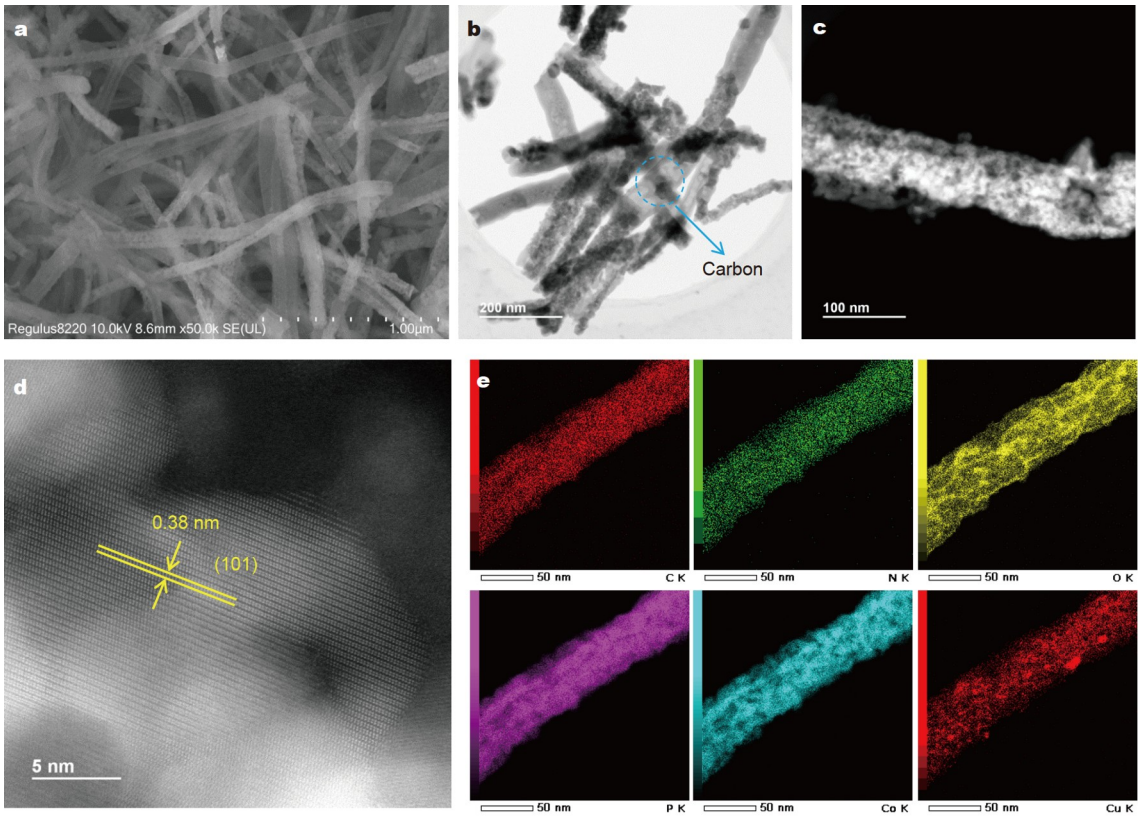

Figure 2 (a) SEM, (b) TEM, (c, d) HAADF-STEM images, and (e) elemental maps of C, N, O, P, Co and Cu in Cu-CoP NFs.

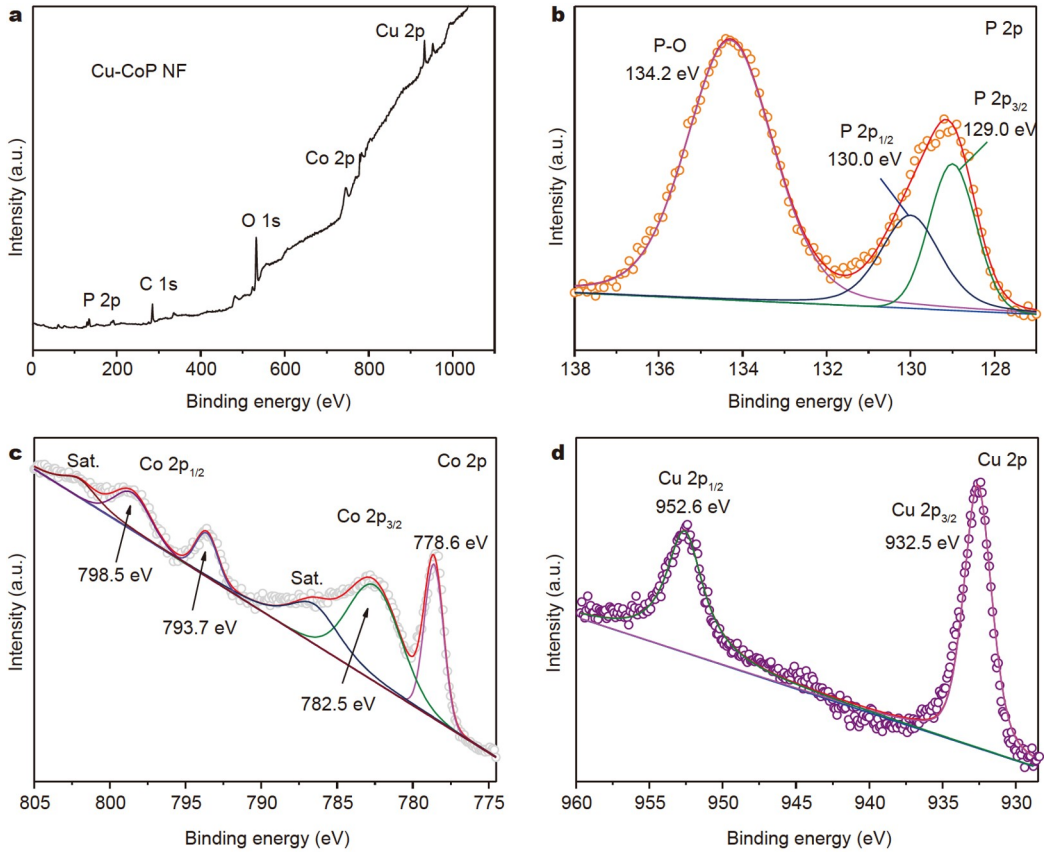

Figure 3 (a) Survey curve, (b) P 2p, (c) Co 2p and (d) Cu 2p spectra of Cu-CoP NFs.

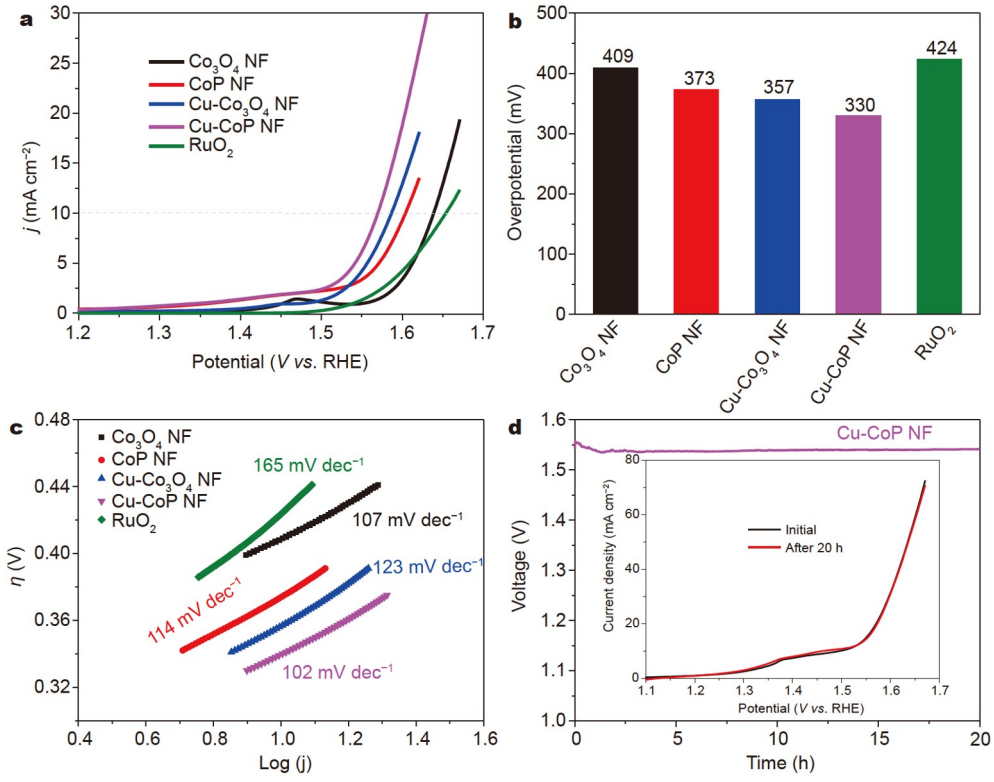

Figure 4 (a) LSV curves, (b) the corresponding overpotential graph, and (c) Tafel slopes of the as-prepared catalysts for OER. (d) Potential change at a stable current density of 10 mA cm^{-2}, with the inset showing LSV curves before and after the stability test.

pared with other catalysts at the same potential, demonstrating the higher density of active sites on the surface (Fig. S11). Additionally, double-layer capacitance (C_{dl}), which is considered to be linearly proportional to the electrochemical surface area (ECSA), was also tested to further understand the density of catalytic active sites [40]. Cu-CoP NFs showed the largest C_{dl} with a value of 10.5 mF cm^{-2}, which is about 1.7 times that of CoP NF (6.1 mF cm^{-2}), 5.5 times that of Cu-Co_3O_4 NFs (1.9 mF cm^{-2}) and more than 6.5 times that of Co_3O_4 NFs (1.6 mF cm^{-2}), demonstrating that Cu-CoP NFs have a much larger ECSA for the catalytic reaction. Although Cu-Co_3O_4 NFs and Co_3O_4 NFs have much higher BET surface areas, their ECSAs are lower than those of Cu-CoP NFs and CoP NFs. This suggests that CoP NFs with a porous structure own more accessible active sites on the surface for OER and the doping of Cu in CoP will further increase their catalytic performances (Figs S12 and S13). Indeed, the reconstructed Co-species at high valences contribute more to OER [41]. The high density of active sites on CoP NFs indicates that the surficial CoP is partially converted into oxidized Co-P species, which are more active than the oxidized Co-O species on the surface of Co_3O_4 [38]. It is easy to understand that Cu-CoP NFs could provide additional active sites for OER, due to the conversion of Cu-P into oxidized Cu-P species during the catalytic process [39]. Of course, when the oxidation process took place on the surface of bulk NFs, the core of NFs still retained the intact structure, resulting in a superb catalytic durability. Thus, Cu-CoP NFs showed the largest ECSA and the best OER catalytic performances.

It should be mentioned that the morphology of nanocatalysts also showed a great influence on catalytic properties. Compared with NFs with a cross-linked structure, CoP NPs and Cu-CoP NPs showed much larger overpotentials with values of 433 and 404 mV, respectively (Figs S14–S16), demonstrating the advantage of this fiber structure. Generally, uniform 1D structures can display a superior conductivity to particle-like materials, attributed to the unique direction for the transfer of electrons. Besides, the superb OER performances of Cu-CoP NFs might also be closely related to the retained carbon or N-doped carbon between metal phosphide NPs. Though these retained carbon species are not the direct active sites for OER, they might also contribute greatly for catalytic reactions such as accelerating the transfer of electrons, and facilitating the release of gases during the reaction [28]. However, too much carbon in the catalysts would deteriorate their catalytic performances. In comparison with Cu-CoP NFs, N-doped porous carbon NFs immobilized with Cu-CoP NPs (NCNF/Cu-CoP) exhibited much lower OER performances under the same testing condition, though their BET surface areas and pore volumes are several times higher than that of Cu-CoP NFs with limited carbon species. This might be because too much carbon will cover part of metal phosphides and decrease the utilization of metal-related active sites (Figs S17–S24). The stability of Cu-CoP NFs was tested at a current density of 10 mA cm^{-2}, which exhibited a stable voltage at 1.54 V over 20 h (Fig. 4d). No obvious changes were observed for LSV curves before and after the stability test, suggesting the excellent OER durability of Cu-CoP NFs in alkaline conditions.

HER

Apart from the superb OER performances, Cu-CoP NFs also showed good HER activity in a 1.0 mol L^{-1} KOH aqueous solution. As shown in Fig. 5, Cu-CoP NFs exhibited an over-

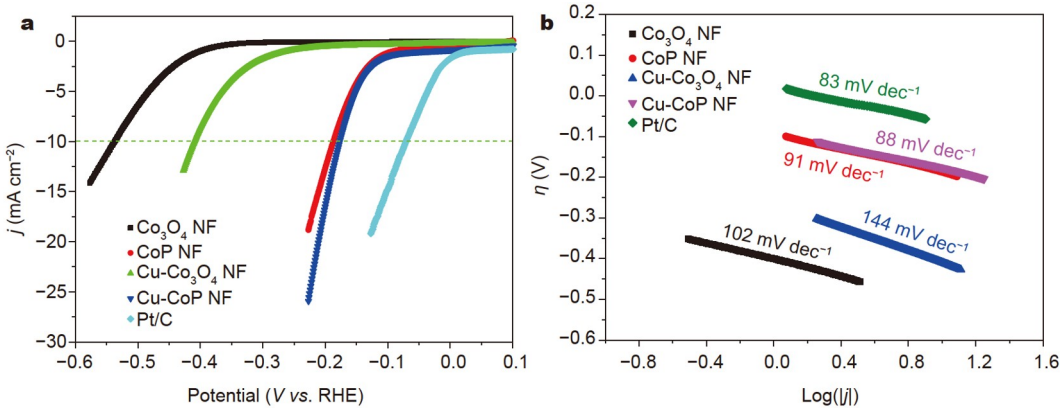

Figure 5 (a) LSV curves and (b) the corresponding Tafel slopes of the as-prepared catalysts for HER.

potential of 176 mV to reach 10 mA cm^{-2} (Fig. S25), lower than those of CoP NFs (186 mV), Cu-CoP NPs (282 mV), and CoP NPs (243 mV), and much superior to those of Cu-Co_3O_4 NFs (409 mV) and Co_3O_4 NFs (537 mV). Though Cu-CoP NFs showed a higher overpotential than commercial Pt/C (70 mV), its Tafel slope was comparable to that of Pt/C nanocatalysts (88 *vs.* 83 mV dec^{-1}) and much lower than that of other samples, indicating the fast HER kinetics on Cu-CoP NFs. The comparable OER performances of Cu-CoP NFs and CoP NFs displayed that Co-related species are the main active sites for the hydrogen evolution process in alkaline conditions. Compared with Cu-CoP NFs, NCNF/Cu-CoP with a high content of carbon exhibited a relatively low activity, further demonstrating the lower density of active sites on the carbon-based nanocatalysts (Fig. S26). Therefore, the control of morphology and active site distributions of nanostructures is essential to the development of functional electrocatalysts.

CONCLUSIONS

Metal phosphide NFs with a diameter of about 100 nm and length of several micrometers were synthesized by using the MOF composite NFs as precursors. The catalytic activity of CoP NFs could be improved by the modulation of Cu species, which efficiently adjusted the electron structure of Co and provided addictional active sites for catalytic reaction. Cu-CoP NFs exhibited superb catalytic performances in alkaline condition for both OER and HER with the overpotentials of 330 and 176 mV, respectively. A limited content of carbon in this kind of nanocatalysts enhanced the catalytic performances, while too much carbon would deteriorate their activity by decreasing the accessible active sites. The outstanding performances of Cu-CoP NFs can be attributed to the fomation of a large catalytic surface area, and the unique 1D porous morphology that facilitates the catalytic reaction. This work provides a facile process to synthesize bifunctional catalysts with desired morphologies and compositions.

Received 14 January 2023; accepted 24 February 2023; published online 9 May 2023

1 Ma TY, Dai S, Jaroniec M, *et al.* Metal-organic framework derived hybrid Co_3O_4-carbon porous nanowire arrays as reversible oxygen evolution electrodes. J Am Chem Soc, 2014, 136: 13925–13931
2 Dai L, Chen ZN, Li L, *et al.* Ultrathin Ni(0)-embedded $Ni(OH)_2$ heterostructured nanosheets with enhanced electrochemical overall water splitting. Adv Mater, 2020, 32: 1906915
3 Zhao CX, Li BQ, Zhao M, *et al.* Precise anionic regulation of NiFe hydroxysulfide assisted by electrochemical reactions for efficient electrocatalysis. Energy Environ Sci, 2020, 13: 1711–1716
4 Wang M, Yang H, Shi J, *et al.* Alloying nickel with molybdenum significantly accelerates alkaline hydrogen electrocatalysis. Angew Chem Int Ed, 2021, 60: 5771–5777
5 Lee Y, Suntivich J, May KJ, *et al.* Synthesis and activities of rutile IrO_2 and RuO_2 nanoparticles for oxygen evolution in acid and alkaline solutions. J Phys Chem Lett, 2012, 3: 399–404
6 Aijaz A, Masa J, Rösler C, *et al.* Co@Co_3O_4 encapsulated in carbon nanotube-grafted nitrogen-doped carbon polyhedra as an advanced bifunctional oxygen electrode. Angew Chem Int Ed, 2016, 55: 4087–4091
7 Kibsgaard J, Tsai C, Chan K, *et al.* Designing an improved transition metal phosphide catalyst for hydrogen evolution using experimental and theoretical trends. Energy Environ Sci, 2015, 8: 3022–3029
8 Li SH, Qi MY, Tang ZR, *et al.* Nanostructured metal phosphides: From controllable synthesis to sustainable catalysis. Chem Soc Rev, 2021, 50: 7539–7586
9 Liu Y, McCue AJ, Li D. Metal phosphides and sulfides in heterogeneous catalysis: Electronic and geometric effects. ACS Catal, 2021, 11: 9102–9127
10 Bodhankar PM, Sarawade PB, Kumar P, *et al.* Nanostructured metal phosphide based catalysts for electrochemical water splitting: A review. Small, 2022, 18: 2107572
11 Li Y, Li H, Cao K, *et al.* Electrospun three dimensional Co/CoP@nitrogen-doped carbon nanofibers network for efficient hydrogen evolution. Energy Storage Mater, 2018, 12: 44–53
12 Tabassum H, Guo W, Meng W, *et al.* Metal-organic frameworks derived cobalt phosphide architecture encapsulated into B/N co-doped graphene nanotubes for all pH value electrochemical hydrogen evolution. Adv Energy Mater, 2017, 7: 1601671
13 Song XZ, Zhao YH, Yang WB, *et al.* Hollow CoP encapsulated in an N-doped carbon nanocage as an efficient bifunctional electrocatalyst for overall water splitting. ACS Appl Nano Mater, 2021, 4: 13450–13458
14 Zou L, Hou CC, Liu Z, *et al.* Superlong single-crystal metal-organic framework nanotubes. J Am Chem Soc, 2018, 140: 15393–15401
15 Li BQ, Zhao CX, Chen S, *et al.* Framework-porphyrin-derived single-atom bifunctional oxygen electrocatalysts and their applications in Zn-air batteries. Adv Mater, 2019, 31: 1900592
16 Qu K, Zheng Y, Zhang X, *et al.* Promotion of electrocatalytic hydrogen evolution reaction on nitrogen-doped carbon nanosheets with secondary heteroatoms. ACS Nano, 2017, 11: 7293–7300
17 Chen G, Wang T, Liu P, *et al.* Promoted oxygen reduction kinetics on nitrogen-doped hierarchically porous carbon by engineering proton-feeding centers. Energy Environ Sci, 2020, 13: 2849–2855
18 Gawande MB, Goswami A, Felpin FX, *et al.* Cu and Cu-based nanoparticles: Synthesis and applications in catalysis. Chem Rev, 2016, 116: 3722–3811

19 Du H, Zhang X, Tan Q, *et al.* A Cu_3P–CoP hybrid nanowire array: A superior electrocatalyst for acidic hydrogen evolution reactions. Chem Commun, 2017, 53: 12012–12015
20 Fu Q, Wu T, Fu G, *et al.* Skutterudite-type ternary $Co_{1-x}Ni_xP_3$ nanoneedle array electrocatalysts for enhanced hydrogen and oxygen evolution. ACS Energy Lett, 2018, 3: 1744–1752
21 Zhang G, Li Y, Xiao X, *et al. In situ* anchoring polymetallic phosphide nanoparticles within porous Prussian blue analogue nanocages for boosting oxygen evolution catalysis. Nano Lett, 2021, 21: 3016–3025
22 Hou CC, Zou L, Wang Y, *et al.* MOF-mediated fabrication of a porous 3D superstructure of carbon nanosheets decorated with ultrafine cobalt phosphide nanoparticles for efficient electrocatalysis and zinc-air batteries. Angew Chem Int Ed, 2020, 59: 21360–21366
23 Zhu R, Chen F, Wang J, *et al.* Multi-channel V-doped CoP hollow nanofibers as high-performance hydrogen evolution reaction electrocatalysts. Nanoscale, 2020, 12: 9144–9151
24 Li J, Li X, Liu P, *et al.* Self-supporting hybrid fiber mats of Cu_3P–Co_2P/N–C endowed with enhanced lithium/sodium ions storage performances. ACS Appl Mater Interfaces, 2019, 11: 11442–11450
25 Salunkhe RR, Kaneti YV, Kim J, *et al.* Nanoarchitectures for metal-organic framework-derived nanoporous carbons toward supercapacitor applications. Acc Chem Res, 2016, 49: 2796–2806
26 Dang S, Zhu QL, Xu Q. Nanomaterials derived from metal-organic frameworks. Nat Rev Mater, 2017, 3: 17075
27 Salunkhe RR, Kaneti YV, Yamauchi Y. Metal-organic framework-derived nanoporous metal oxides toward supercapacitor applications: Progress and prospects. ACS Nano, 2017, 11: 5293–5308
28 Wei YS, Zhang M, Kitta M, *et al.* A single-crystal open-capsule metal-organic framework. J Am Chem Soc, 2019, 141: 7906–7916
29 Cai G, Zhang W, Jiao L, *et al.* Template-directed growth of well-aligned MOF arrays and derived self-supporting electrodes for water splitting. Chem, 2017, 2: 791–802
30 Chen H, Shen K, Mao Q, *et al.* Nanoreactor of MOF-derived yolk-shell Co@C–N: Precisely controllable structure and enhanced catalytic activity. ACS Catal, 2018, 8: 1417–1426
31 He B, Zhang Q, Pan Z, *et al.* Freestanding metal-organic frameworks and their derivatives: An emerging platform for electrochemical energy storage and conversion. Chem Rev, 2022, 122: 10087–10125
32 Wang Q, Astruc D. State of the art and prospects in metal-organic framework (MOF)-based and MOF-derived nanocatalysis. Chem Rev, 2019, 120: 1438–1511
33 Ding D, Shen K, Chen X, *et al.* Multi-level architecture optimization of MOF-templated Co-based nanoparticles embedded in hollow N-doped carbon polyhedra for efficient OER and ORR. ACS Catal, 2018, 8: 7879–7888
34 Lin Y, Yang L, Zhang Y, *et al.* Defective carbon-CoP nanoparticles hybrids with interfacial charges polarization for efficient bifunctional oxygen electrocatalysis. Adv Energy Mater, 2018, 8: 1703623
35 Cao E, Chen Z, Wu H, *et al.* Boron-induced electronic-structure reformation of CoP nanoparticles drives enhanced pH-universal hydrogen evolution. Angew Chem Int Ed, 2020, 59: 4154–4160
36 Zhou YN, Yu WL, Cao YN, *et al.* S-doped nickel-iron hydroxides synthesized by room-temperature electrochemical activation for efficient oxygen evolution. Appl Catal B-Environ, 2021, 292: 120150
37 Mei G, Liang H, Wei B, *et al.* Bimetallic MnCo selenide yolk shell structures for efficient overall water splitting. Electrochim Acta, 2018, 290: 82–89
38 Hou CC, Cao S, Fu WF, *et al.* Ultrafine CoP nanoparticles supported on carbon nanotubes as highly active electrocatalyst for both oxygen and hydrogen evolution in basic media. ACS Appl Mater Interfaces, 2015, 7: 28412–28419
39 Hou CC, Chen QQ, Wang CJ, *et al.* Self-supported cedarlike semimetallic Cu_3P nanoarrays as a 3D high-performance Janus electrode for both oxygen and hydrogen evolution under basic conditions. ACS Appl Mater Interfaces, 2016, 8: 23037–23048
40 Fan J, Zhao X, Mao X, *et al.* Large-area vertically aligned bismuthene nanosheet arrays from galvanic replacement reaction for efficient electrochemical CO_2 conversion. Adv Mater, 2021, 33: 2100910
41 Zeng Y, Zhao M, Huang Z, *et al.* Surface reconstruction of water splitting electrocatalysts. Adv Energy Mater, 2022, 12: 2201713

Acknowledgements This work was financially supported by the National Institute of Advanced Industrial Science and Technology (AIST), Jiangsu University (4023000046), Shenzhen Key Laboratory of Micro/Nano-Porous Functional Materials (SKLPM) (ZDSYS20210709112802010), China Postdoctoral Science Foundation (2022TQ0126 and 2022M721375), Guangdong Grants (2021ZT09C064), and the National Key Research and Development Project (2022YFA1503900).

Author contributions Zou L, Wei YS, Xu Q and Kitagawa S conceived the project and designed the experiments. Zou L fabricated the samples, tested the physical and electrochemical performances of the nanocatalysts and wrote the manuscript. Wang Q performed the XPS analysis and revised the manuscript. Liu Z was responsible for the TEM analysis. All authors analyzed the data and contributed to the discussion.

Conflict of interest The authors declare that they have no conflict of interest.

Supplementary information Experimental details and supporting data are available in the online version of the paper.

Lianli Zou received his PhD degree in 2019 from Kobe University under the supervision of Prof. Qiang Xu. After working as a postdoctoral researcher at AIST-Kyoto University CHEM-OIL, he jointed Jiangsu University in 2021 and worked as an assistant professor. His research interests are focusing on the synthesis and application of low-dimensional nanomaterials for catalysis and energy storage.

Qiang Xu received his PhD degree from Osaka University in 1994. He worked as the director of AIST-Kyoto University CHEM-OIL, adjunct professor of Kobe University/Kyoto University, and is now chair professor of Southern University of Science and Technology. His research interests include the chemistry of nanostructured materials and their applications, especially for catalysis and energy.

Susumu Kitagawa obtained a PhD degree from Kyoto University. He is a distinguished professor and director of iCeMS, Kyoto University. He initiated the science and technology of gas with porous coordination polymers (PCPs) and metal-organic frameworks (MOFs). He pioneered the chemistry of flexible PCPs/MOFs and named soft porous crystals (SPCs), demonstrating various functions such as storage and separation. He classifies this material as Generations I to IV as it develops.

MOF衍生的磷化钴纳米纤维用于电催化氧析出和氢析出反应

邹联力[1,4], 魏永生[1], 王秋菊[4], 刘铮[2], 徐强[1,3,5*], Susumu Kitagawa[1,3*]

摘要 高性能催化剂的开发和利用是能源领域的研究热点，其中制备具有高活性面积的一维纳米催化剂是目前的难点. 本研究以金属有机框架(MOF)复合纤维为前驱体，通过热处理-磷化过程制备了具有氧析出(OER)和氢析出(HER)双功能特性的CoP纳米纤维. 该MOF衍生策略也可以用来制备其他一维纳米材料，如Co_3O_4纳米纤维、Co/C纤维和CoP/C复合纤维. 研究表明，CoP纳米纤维的直径约100 nm，长度可达几微米，具有较高的活性面积. 通过Cu掺杂改性可以提高CoP纳米纤维的催化活性，碱性条件下测得其对OER和HER的过电位分别为330和170 mV，可与商业的贵金属催化剂相媲美. 该工作也为一维双功能电极催化剂的制备及功能化提供了研究基础.